Available online at www.sciencedirect.com
SCIENCE DIRECT®
Journal of Inorganic Biochemistry 99 (2005) 1126–1134
Journal of Inorganic Biochemistry
www.elsevier.com/locate/jinorgbio

Racemic D,L-[Co(phen)$_2$dpq]$^{3+}$–DNA interactions: Investigation into the basis for minor-groove binding and recognition

Yanbo Wu, Huili Chen, Pin Yang *, Zhenhai Xiong

Institute of Molecular Science, Key Laboratory of Chemical Biology and Molecular Engineering of Ministry of Education, Shanxi University, Taiyuan 030006, PR China

Received 19 November 2004; received in revised form 7 February 2005; accepted 10 February 2005
Available online 19 March 2005

Abstract

A study on the minor-groove recognition of B-DNA d(GTCGAC)$_2$ by racemic D,L-[Co(phen)$_2$dpq]$^{3+}$, where phen and dpq stand for 1,10-phenanthroline and dipyrido [3,2-d:2,3-f]quinoxaline, respectively, was carried out with a one-, two-dimensional (1D, 2D) nuclear magnetic resonance (NMR) methodologies and molecular simulations. NMR investigations revealed that the metal complex intercalates into the DNA base stack from minor groove orientation with dpq as intercalator and dpq ligand participated in the nucleobase stack. Molecular docking simulations of these systems were consistent with the experimental results and revealed that the recognition shows obvious enantioselectivity: the L-isomer is favored at the pyrimidine–purine/purine–pyrimidine region, especially CG/GC sequence, while the D-isomer is favored at the pyrimidine–pyrimidine/purine–purine region, especially TC/AG sequence. Surprisingly, we found that the L-isomer would be enriched when racemic complex was employed. So contrary to general viewpoint, the L-isomer of complex recognized this right hand double helical DNA preferentially. Detailed analysis suggests that it is the electrostatic interactions that determine the steric interactions and then determine the whole recognition event.

Keywords: Racemic metal complex; DNA recognition; NMR; Molecular simulation

1. Introduction

Metal complexes in general form (M(phen)$_2$L]$^{n+}$ [where M is transition-metal ions, ancillary ligand phen (1,10-phenanthroline) could be replaced by bidentate ligand such as phi (9,10-phenanthrenequinone diimine), bpy (2,2′-bipyridyl), etc, and bidentate ligand L has a planar aromatic heterocyclic functionality that can insert and stack between the base pairs of double helical DNA) have contributed to our understanding of fundamental nucleic acid recognition. These metal complexes have been applied in the development of DNA cleavage reagents, have assisted in the development of low molecular weight drugs, and as stand-alone metal complexes, have been agents to understand fundamental complex interactions with DNA [1–9]. In the last area, intercalation of ligand L into DNA base stack has been emphasized on enantioselectivity, site-specificity and binding mechanism, etc. [10–15]. So far, most studies are limited to spectroscopy methods [4–6,16–20]. However, it is difficult to clarify the details of the interaction by the phenomenological information, such as red shift, blue shift, hyperchromicity, hypochromicity, etc. So some more accurate methods, such as two dimensional (2D) NMR spectrum, etc., were used to describe the interaction between DNA and some metal complex that could be separated into their stable enantiomers [9,11–14], and a large number of details have been acquired. However, for other complexes, such as some cobalt complexes, the separated isomers will racemize rapidly in the presence of oligonucleotide to generate a stable mixture of

* Corresponding author. Tel./fax: +86 3517011022.
E-mail address: yangpin@sxu.edu.cn (P. Yang).

0162-0134/$ - see front matter © 2005 Elsevier Inc. All rights reserved.
doi:10.1016/j.jinorgbio.2005.02.008

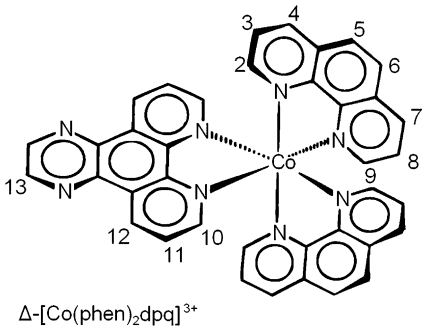

Fig. 1. D-$[Co(phen)_2dpq]^{3+}$.

enantiomers enriched in the isomer that interacts most favorably with the oligonucleotide [15]. When these kinds of racemic complexes were employed, it would be very interesting to know interactive details of their binding with ODN. However, it is difficult to acquire corresponding information only by experimental investigations, and this lead to a situation that our knowledge about the interactions of nucleic acid recognition is relatively poor. In view of the above situation, the present study stresses on the mode and mechanism of racemic metal complexes–DNA-binding interactions with the combination of theoretical and experimental methods.

As a good intercalator, bidentate ligand dipyrido [3,2-d:2,3-f]quinoxaline (dpq) has been employed in investigations of the interaction between oligodeoxynucleotide (ODN) and separatable $[Ru(phen)_2dpq]^{2+}$ [9], while the binding of complex $[Co(phen)_2dpq]^{3+}$ to DNA has not been reported so far. In this paper, we first studied the interaction between racemic D,L-$[Co(phen)_2dpq]^{3+}$ and ODN $d(GTCGAC)_2$ through two methods, i.e., 2D NMR and molecular modeling in a complementary way. The titled complex is shown in Fig. 1.

2. Experimental

2.1. Materials

The metal complex was synthesized with the method reported [21] and the ODN $d(GCGAGC)_2$ was purchased from AuGCT Biotechnology Co. Ltd, Beijing. The concentration of ODN was determined from the absorbance at 260 nm. It was dissolved in 0.50 ml of 10 mM-phosphate buffer (pH 7.0), containing 20 mM NaCl and 0.05 mM 3-trimethylsilyl-[2,2,3,3-D4]propionate (TMSP). For studies on protons on imino group, the sample was dissolved into 90%H_2O/10%D_2O, While for non-exchangeable proton studies, the sample was repeatedly lyophilized for 3 times from 99.8% D_2O in a speed vacuum, and then dissolved in 0.50 ml 99.996% D_2O. Stock solution of the metal complexes was prepared in D_2O (unbuffered) and added to the hexanucleotide in 10 μl aliquots until a metal complex to hexanucleotide duplex ratio (R) of 1 was achieved.

2.2. NMR measurements

NMR measurements were made on Bruker DRX-500 and DRX-300 spectrometers and analyzed on silicon graphics workstation by Xwin-NMR software package. Proton chemical shifts were referenced to an internal TMSP standard.

All NMR experiments were carried out under room temperature, at approximately 20 °C. Spectra recorded in 90%H_2O/10%D_2O were collected using a binomial 1:3:3:1 pulse sequence for HDO peak suppression. Phase sensitive Nuclear Overhauser and Enhancement Spectroscopy (NOESY) spectra in 99.996% D_2O were recorded by the Time Proportional Phase Incrementation (TPPI) method using 2048 data points in t_2 (over a spectral width of 5000 Hz) for 256 $t_1$values with a pulse repetition delay 2 s with 80 scans per fid. To acquire more information that could be investigated in complementary way with molecular simulations, a mixing time of 350 ms was adopted. Suppression of the residual HDO resonance was achieved by low-power presaturation during the relaxation delay. Two-dimensional NMR data sets were zero-filled to 1024 points in the t_1 dimension and apodized with shifted sinebell function.

2.3. Molecular modeling and simulations

All calculations were performed on the Silicon Graphics workstation with insight II software packages. Default settings for that program were used unless specified otherwise. The coordination complex contains a cobalt atom with an octahedral coordination structure. Extended Systematic Force Field (ESFF) could deal with both ODN and metal complex simultaneously, and give out relative more output information for analysis, so the default ESFF force field parameters were used.

Electroneutrality of each docked structure was achieved with the addition of 17 Na^+ counterions by standard procedures to balance the 10 phosphate anions provided by each single strand of DNA and the positively charged metal complex. At the beginning of optimization and energy minimization, the Steepest Descent method was used until the Root mean square (RMS) deviation was less than 5.0 kcal/mol. Then it was switched to Conjugate Gradient method automatically by the DISCOVER 98 program. When the RMS deviation was less than 0.5 kcal/mol, optimization and energy minimization was stopped.

3. Results and analyses

3.1. NMR measurements

3.1.1. 1D NMR investigations

Qualitative NMR studies were pursued to understand the binding location and orientation of the racemic metal complex upon ODN association. Fig. 2 and some figure in supporting information show the 1D spectra for racemic $[Co(phen)_2dpq]^{3+}$ and ODN 1:1, as well as the spectra of $[Co(phen)_2dpq]^{3+}$ and ODN alone. As shown in the spectra, some changes upon the titration were immediately evident. Firstly, $T_2 \cdot A_5$ and $C_3 \cdot G_4$ base pair imino proton resonances (supporting information) broadened greatly with up-field movements, which suggest that one of the aromatic ligand maybe located in the base stack. The G1. C6 base-pair imino resonances at the termini of the ODN, extensively exchange broadened due to their location, were not observed, as was reported previously [9].

Secondly, as shown in Fig. 2, obvious chemical shift changes of H12 and H13 on ligand dpq, more specifically, the values of D move from 9.96 and 9.39 ppm to 9.14 and 8.76 ppm, respectively, while the chemical shift changes of 0.05–0.20 ppm for phen protons resonance indicates that the dpq ligand interacts preferentially with the ODN. Moreover, the extent and orientation of chemical shift changes reveal that ligand dpq intercalates into base stack selectively [9,12,22]. Due to the limitation of NMR devices, we could not distinguish H2 of ancillary ligand phen from H9, H3 from H8, H4 from H7, and H5 from H6, these protons were marked as H5/6, H4/7, H3/8, and H2/9, respectively.

Thirdly, as titration went on, the major groove protons, such as H6/H8 protons from the bases, only broadened slightly, which means that the major groove was much less affected. While for the protons in the minor groove, such as the deoxyribose protons H1′ and H2′, their Ds were broadened notably, together with certain shifts, which indicates that the minor groove was affected greatly (supporting information). We think that, from the aforesaid 1D NMR studies, the racemic metal complex should intercalate between DNA bases from the minor groove by taking dpq as the intercalator.

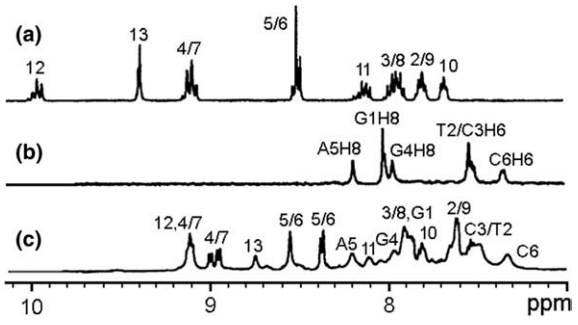

Fig. 2. ^{1}H NMR spectra: (a) free complex, (b) free oligodeoxynucleotide and (c) added complex into oligodeoxynucleotide system.

3.1.2. 2D NMR investigations

In addition to 1D experiments, 2D experiments were also recorded. At first, a spectrum of duplex 5′-(GTC-GAC)$_2$-3′ without the addition of metal complex was generated at 20 °C (Fig. 3) as the reference. Upon the titration with metal complex, the sequential cross-peaks stemmed from ODN varied and broadened greatly, indicating extensive interactions between ODN and metal complex. This agrees with the result form 1D experiment. Upon the titration of metal complex, many cross-peaks appeared in the NOESY spectra (Fig. 4). These peaks originated mainly from the Nuclear Overhauser Effect (NOE) between protons in the minor groove and protons of ancillary ligand phen, such as H5/6-A_5H1′, H2/9-G_4H1′, H2/9-T_2H1′, etc. Worthy of note, a moderate-intensity NOE cross-peak for the major groove T_2 methyl and dpq-H13 proton intermolecular interactions was observed at 8.30 by 1.37 ppm (see Fig. 4 and an expansion of that region in Fig. 5),

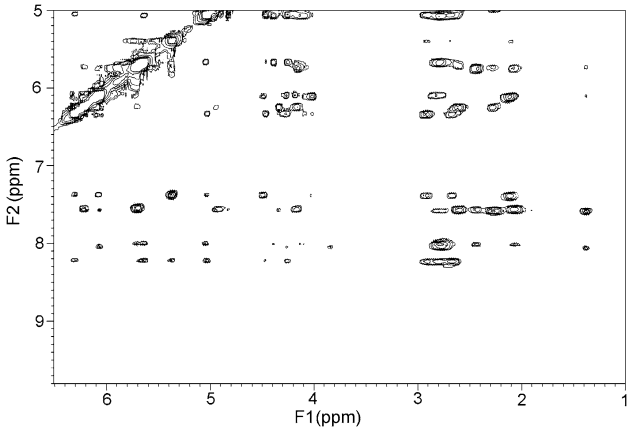

Fig. 3. NOESY spectra of free oligodeoxynucleotide.

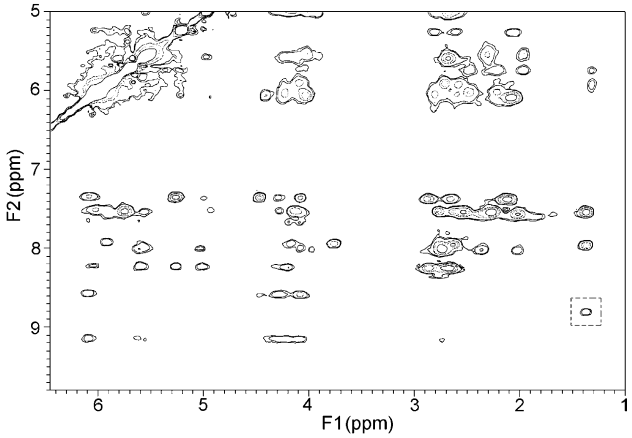

Fig. 4. NOESY spectra of oligodeoxynucleotide: complex = 1:1.

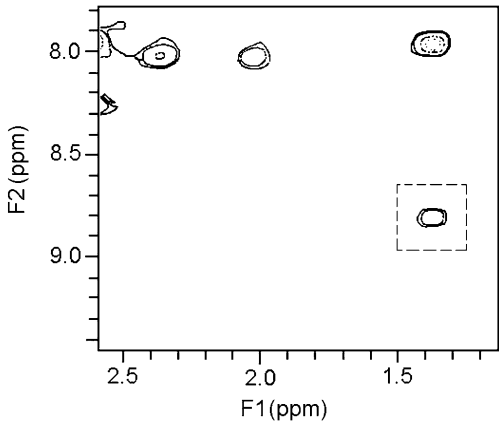

Fig. 5. Enlargement of the region around T_2 methyl-H13 cross-peak seen in Fig. 4.

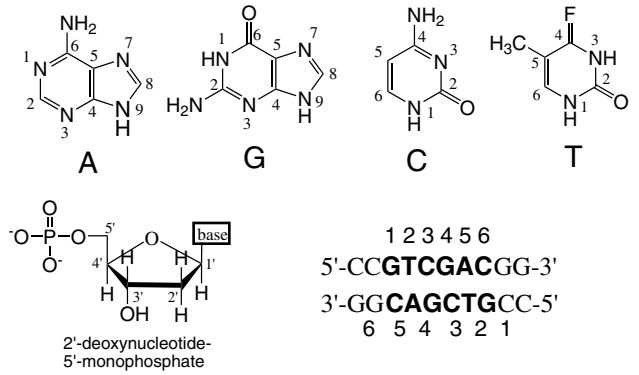

Fig. 6. Nucleobase, deoxyribose and the DNA sequence used in this work.

indicating the forepart of the dpq has already located at the major groove side. All the information described above, taken together, shows that the dpq ligand of complex intercalated into the DNA base stack from the minor groove and strode across the bases from the minor groove to the major groove.

From our above experimental information we infer that the metal complex intercalates into the nucleobase stack from minor groove by taking dpq ligand as its intercalator and then stabilizes the stacking. However, the use of racemic complex and the conversion between its isomers complicated the interactions so much so that the differentiation ability of up-to-date NMR devices was not adequate to deal independently with it. Especially, we could not investigate the enantioselectivity of interactions by NMR studies alone. So the experimental results described above will be analysed in a complementary way with following theoretical investigations.

3.2. Molecular modeling and simulations

To acquire the detailed binding information, we carried out a computational examination of Co (III) complex interacting with the ODN by using molecular modeling and simulation. As a starting point for these investigations, the ODN $d(CCGTCGACGG)_2$ (Fig. 6) was constructed in the BIOPOLYMER module. Considering the terminal effect, two base pairs were added on each end of the ODN. Geometry and energy minimizing optimizations were undergone in Assisted Model Building and Energy Refinement (AMBER) force field, and then the atom types and charges were redefined automatically by ESFF force field. The two isomers of metal complex were constructed in BUILDER module. Geometry and energy minimizing optimizations were carried out in ESFF force field.

Each isomer was docked manually into the DNA base stack between every double base pairs except the later-added CC/GG and CG/GC region on the each end, and intercalations were undergone in the major groove and minor groove, respectively. Significantly, the docked starting structures were generated independently of the 1D and 2D NMR data described earlier. Constraints based on observed NOEs were not used in generation of the starting structures, nor were any constraints employed during the course of the modeling and simulations. As a beginning, the dpq plane was placed nearly parallel to the base pairs plane (perpendicular to DNA helix axis) and just out of the DNA helix (Fig. 7-1). This point was regarded as the first checkpoint and its intercalation depth was defined as 0. Then, Co (III) complex was docked into base stack until the dpq ligand was intercalated into the base stack entirely (Fig. 7-2). The length of inserting step, i.e. the distance between neighboring checkpoints was 2 Å, and the intercalation depths were thus defined as 2 Å, 4 Å..., etc. Simulations of all systems containing ODN were carried out in aqueous solution, while other systems in vacuum.

The calculation results were listed in the supporting information. With analysis of the data we found that

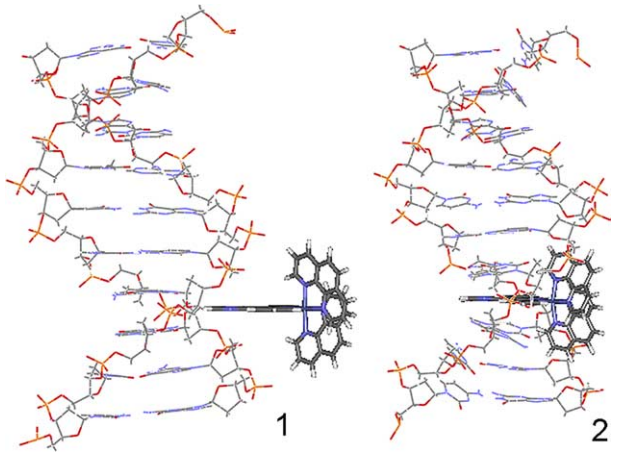

Fig. 7. (1) Location of complex and ODN before intercalation. (2) Insert into the base stack entirely.

the intercalation of D-isomer in the T_2C_3/A_5G_4 region ($E = 2606.38$ kcal/mol) and that of L-isomer in the C_3G_4/G_4C_3 region ($E = 2595.10$ kcal/mol) were the most preferential acting mode. Significantly, the two recognizing intercalations were all occurred in the minor groove, which was correspondence to the NMR results described above. Due to distinction of potential energy, the L-isomer-ODN association is more stable than that of D-isomer, we conjecture, referred to the result of Rehmann and Barton [15], that the L-isomer may be enriched when the complex interacts with oligonucleotide. And the interaction of L-isomer upon ODN association will affect the experimental behaviors of the whole system mostly, such as the intensity of cross-peaks in the NOESY spectra.

3.3. Simulations assisted cross-peaks assignment

Shown in Fig. 8 are cross-peaks assigned in this work. The easily assigned peaks are as the follows: The cross-peak of H13-T_2CH_3 intermolecular NOE appeared at 1.37 by 8.78 ppm, the interactions between C_3H1', G_4H1', A_5H1', G_4H2'' protons and H4/7 generated cross-peaks at 5.57, 5.62, 6.10 and 2.72 by 9.12 ppm, respectively, the cross-peak of H5/6-A_5H1' appeared at 6.18 by 5.56 ppm and the cross-peaks of H2/9-C6H1′, G4H1′ intermolecular NOEs appeared respectively at 6.10 and 5.60 by 7.63 ppm. As other cross-peaks in the spectra could not be assigned clearly, we picked up the two optimal models acquired by molecular simulations to assist the assignment of cross-peaks through contrasting the intensity of peaks in the spectra with the corresponding distances between concerned protons in the optimal models. Initially, those distances of protons concerning clear-assigned cross-peaks are listed in the Table 1. According with the simulation presumptions above, the distances measured in the L-isomer's intercalation mode were consistent with the intensity of corresponding peaks, while the distances of concerned protons in the intercalation model of D-isomer-ODN association were deviated greatly from the corresponding intensity of cross-peaks, which reveals that *the interactions of L-isomer-ODN association influence the overall NMR behaviors of the system mostly*. Furthermore, the intensity of the peaks generated independently by D-isomer-ODN intermolecular NOEs was much weaker than that the distances should have corresponded to, *suggesting the puny interaction mode*.

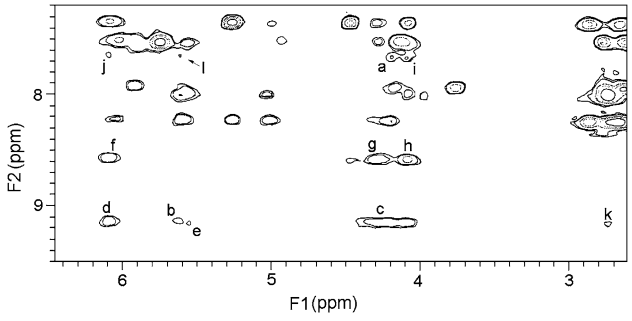

Fig. 8. Enlargement of the region around the phenanthroline protons-minor groove protons intermolecular cross-peak seen in Fig. 4.

As molecular simulations explained the clear-designed cross-peaks in the NOESY spectra properly, it is reasonable to use the optimal models to assign indistinct cross-peaks in the spectra and search the potential NOEs through the measure of the distances between some protons in the optimal models. Results revealed that the intensity of the newly assigned cross-peaks were also affected mainly by L-isomer–ODN interactions, which accorded with the results above. All the newly assigned peaks are listed in Table 2.

Investigating the attribution of cross-peaks, we found that the interaction of D-isomer in T_2C_3 region to generate more NOEs than that of L-isomer in the C_3G_4 region. We attribute this to the symmetrical character of the ODN, more specifically, owing to the asymmetry of T_2C_3 region and to the symmetry of C_3G_4 region, the metal complex protons are more favorable to act with more kinds of ODN protons when the D-isomer intercalated into the former's T_2C_3 region than the

Table 1
Contrast of the corresponding distance with the intensity

Protons	Peaks	D-isomer in T_2C_3/A_5G_4 region		L-isomer in C_3G_4/G_4C_3 region	
		Corresponding distances	Rationality	Corresponding distances	Rationality
H13-T_2CH_3	Fig. 5(m)[a]	2.77/3.65/4.38/4.94/5.34	×	4.33/4.42/4.49/5.05/5.36/5.94	√
H4/7-C_3H1'	e[b](w)	3.72	×	–	–
H4/7-G_4H1'	b(w)	2.96	×	4.18/4.33	√
H4/7-G_4H2'	k(w)	3.38	×	4.85/5.04	√
H4/7-A_5H1'	d(s)	3.83/4.87	×	3.25/3.46/5.20/5.59	√
H5/6-A_5H1'	f(s)	3.72	×	2.79/3.31/3.70/4.32	√
H2/9-C_6H1'	j(w)	3.66/4.28	×	–	–
H2/9-G_4H1'	l(vw)	3.42/4.14	×	4.44/4.62	A little bigger

[a] s = strong, m = moderate, w = weak and vw = very weak.
[b] Letters correspond the peaks in Fig. 8.

Table 2
The assigned cross-peaks

Peaks	Possible protons to bring this peak	
	D-isomer in T_2C_3 region	L-isomer in C_3G_4 region
Fig. 5	H13-T_2CH_3	H13-T_2CH_3
a*	H2/9- A_5 H4′/H5′	–
b	H4/7-G_4H1′	H4/7-G_4H1′
c	H4/7-G_4H4′, H4/7-A_5H4′/H5′	H4/7-G_4H4′, H4/7-A_5H4′/H5′
d	H4/7-A_5H1′, H5/6- C_3H4′/H5′	H4/7-A_5 H1′
e	H4/7-C_3H1′	–
f	H5/6-T_2H1′	H5/6-A_5H1′
g	–	H5/6-G_4H4′
h	H5/6-A_5H4′/H5′	H5/6-A_5H4′/H5′
i	H5/6-C_3H4′/H5′, H2/9-G_4H4′/H5′	–
j	H2/9-C_6H5′, H2/9-C_6 H1′	–
k	–	H4/7-G_4H2′
l	–	H2/9-G_4H1′

* Letters "a"→"l" correspond the peaks in the Fig. 8.

L-isomer intercalated into the later's C_3G_4 region. Accordingly, the former will generate more kinds of cross-peaks.

In summary, the NMR investigations show the acting mode and interaction orientation, while the molecular simulations offer the accurate interaction site for each isomer and point out the preponderant isomer. Moreover, the analyses about intensity of cross-peaks show that the interactions of L-isomer-ODN association influence the overall NMR behaviors of the system mostly, which was close corresponding to the simulation conjecture that the L-isomer will be enriched when racemic $[Co(phen)_2dpq]^{3+}$ interacts with this ODN. This indicates that the theoretical method is reliable. So it is feasible that the detailed analyses were based mainly on the simulation results. Worthy of note, those analyses were not only consisted with the viewpoints described above, but also offered us the further knowledge of the racemic metal complex–ODN interactions.

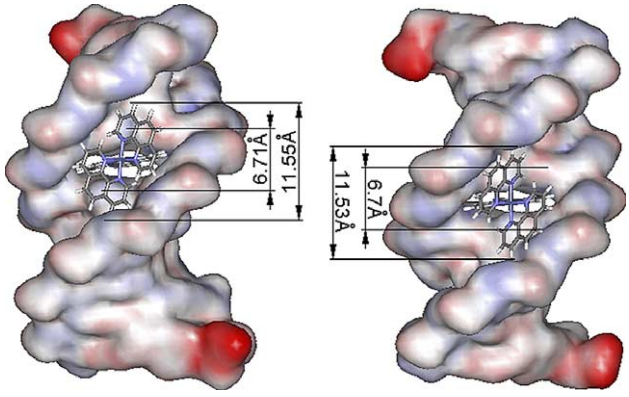

Fig. 9. The optimal state of intercalation, left: D-form in T_2C_3 region, right: L-form in C_3G_4 region.

4. Discussion

4.1. Structure of ODN–complex association

Though the size of dpq was only about 8 Å, due to the movement of nucleobases to major groove, the expanding of the ODN side chain and the hydrophobe cavity formed at the end of the intercalation, both isomers had moved to major groove orientation for 14 Å in their recognition site compared to their original location. As shown in Fig. 9, the interactions make the dpq ligand of the metal complex stay at the base stack, while the ancillary ligand phens stay at the hydrophobe cavity in the minor groove. These structures are very stable. When ligand dpq entered between the base pairs, the corresponding distances of base pairs were increasing from standard 3.4 Å to about 6.7 Å, which were almost doubled. The distance between the dpq and base pairs was about 3.35 Å, which was very similar to the distance between the standard base pairs. Moreover, the depths of the intercalation for both enantiomers of the complex were all 14 Å in their recognition sites, which together with the structural characters of the dpq-base pairs association showed that the dpq ligand participated in the nucleobase stack stably.

In addition, the stretched sizes of ancillary ligand phenanthroline were 11.55 Å for D-isomer and 11.53 Å for L-isomer (Fig. 9), which were both much larger than the standard distance of 3.4 Å between the neighboring nucleobase pairs. When ligand dpq stacked in ODN bases, the ancillary ligand phen will interact with ODN minor groove region corresponding to 4–6 base pairs around the recognition site, which maybe generate the NOEs between protons on them. In other words, the considerable cross-peaks concerning those non-recognition site maybe appeared in the NOESY spectra. This was close corresponding to the results in Table 2.

4.2. Enantioselectivity

In our study, the racemic metal complex was used in NMR investigations. Still, enantioselectivity could be investigated with the aid of molecular simulations. Surprisingly, L-isomer of complex will preferentially recognize the right hand double helical structure of the ODN.

Considering the structural characters of the complex and its recognition regions, the authors think that the steric interaction is the crucial factor. With four Watson–Crick bases, purine bases A and G are larger than pyrimidine base C and T, so purine base will bring more steric collisions than pyrimidine base when the metal complex intercalated into ODN base stack. Take the situation in the C_3G_4/G_4C_3 and T_2C_3/A_5G_4 regions for example, when complex collides with nucleobases in the C_3G_4/G_4C_3 region, the ancillary ligand phen of L-isomer faces pyrimidine base G (Fig. 10-1), while the phen of D-isomer faces purine base C (Fig. 10-2). Obviously, L-isomer's binding is preferential due to the minor steric collisions. When the complex intercalates the T_2C_3/A_5G_4 region, both isomers have one ancillary ligand phen that collides with purine base and the other collides with pyrimidine base. In this condition, the D-isomer fits the right hand conformation. Therefore, D-isomer's binding is preferential in the T_2C_3/A_5G_4 region.

With the discussion above, the authors extrapolated the enantioselectivity to a broad sense: the D-isomer of the complex recognizes the pyrimidine–pyrimidine/purine–purine region, and L-isomer recognizes the pyrimidine–purine/purine–pyrimidine region.

4.3. Groove selectivity

Consisted with our previous simulating studies of interactions between metal complex and normal sequence DNA [23–25], the optimal interaction events occurred in the minor groove and the intercalations from minor groove were generally more preferential than that from major groove. To explain the groove selectivity, the optimal models were analyzed and the steric interactions were once again found to be the determinant. As shown in Fig. 11(a), when the intercalation starts from the major groove, nucleobases have to move toward the close-constructed minor groove region due to steric hindrance that makes the base pairs crowding (arrow 1). At the same time, to accommodate the complex, the intercalation will be accompanied by structural distension (arrow 1′) of the side chain, which was limited by a counterforce of whole ODN (arrow 1′). When the intercalation started from minor groove, as shown in Fig. 11(b), the nucleobases will move to open-constructed major groove region (arrow 2), and there have few structural limitations to the distension (arrow 2′) of ODN side chain. So the intercalation from the major groove will encounter more steric collision

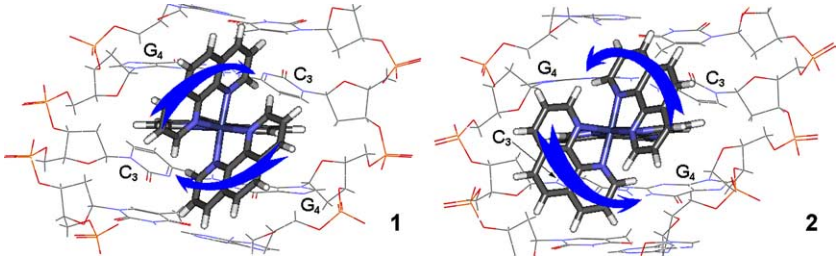

Fig. 10. (1) The comparison of intercalation of L-form (1) and D-form (2) in C_3G_4 region in the minor groove. Arrows point to the bases colliding with the phenanthroline.

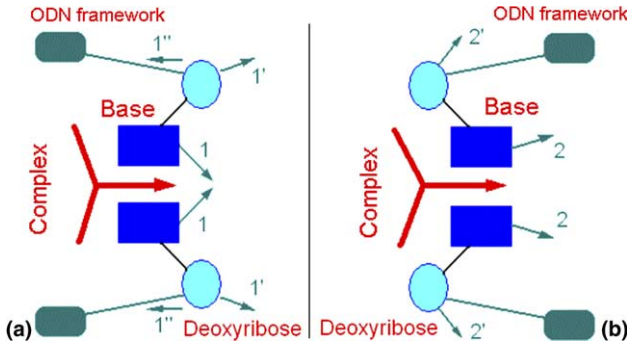

Fig. 11. The intercalation from the major groove (a) and from the minor groove (b).

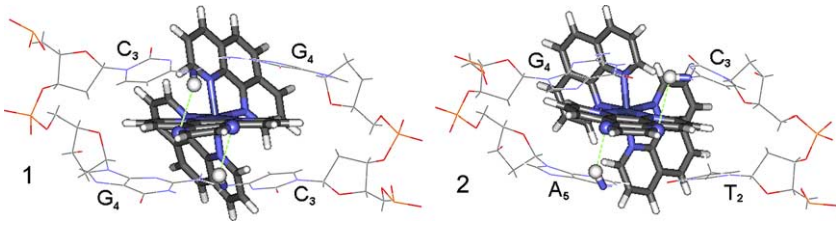

Fig. 12. New-formed H-bonds: (1) L-form in C_3G_4 region and (2) L-form in T_2C_3 region.

Table 3
Detailed energy (kcal/mol) comparison of optimal interaction style

Items	D-isomer in			L-isomer in		
	G_1T_2	T_2C_3	C_3G_4	G_1T_2	T_2C_3	C_3G_4
Total	2655.02	**2606.38**	2615.15	2672.04	2616.48	**2595.10**
Internal	658.64	644.42	647.65	670.52	654.27	654.90
Non-bond	1996.38	1961.96	1967.49	2001.52	1962.21	1940.20
VDW	10.76	18.92	14.57	7.14	9.86	25.67
Elect	1985.62	1943.04	1952.92	1994.38	1952.34	1914.53

than that from the minor groove. Consistent with the analyses above, the energy distribution (supporting information) shows that the intercalation depths were deeper and the potential energies were lower in the minor groove than in the major groove, indicating a much facile binding interactions in the minor groove.

So we conclude that it is the structural differences of the different ODN regions that lead to the different steric conflict during the binding and makes the recognition courses show enantio-selectivity and groove-selectivity. In a word, steric interaction is the determinant.

4.4. Hydrogen bonds

We also investigated the hydrogen bonds formed during docking processes and we found that, in the intercalation of L-isomer in C_3G_4 region, the amido hydrogens of C_3 were in close proximity to the prominent H-bond acceptor, pyrazine N of dpq ligand, so two hydrogen bonds were formed in the symmetrical system during the simulation. With the intercalation of D-isomer in T_2C_3 region, there also had two H-bonds formed in the intercalating process, namely, the amido hydrogens of C_3 and A_5 formed bonds respectively to pyrazine N of dpq ligand (Fig. 12). Those new-formed hydrogen bonds stabilized the optimal structures. And in other mode, no new hydrogen bond was formed.

4.5. Electrostatic interactions

Consistent with the former work of our laboratory [24–26], electrostatic interactions play an important role in the interaction process. The subentry of the total energy of each site in the minor groove obtained by simulation was investigated in detail (Table 3). In the table, Total means total energy; VDW means Van de Waals energy; Elect means electrostatic energy; Non-bond means non-bond energy (the sum of the VDW and electrostatic energy), which describes the steric interaction; Internal means internal energy, which describes the bond properties. As shown in Table 3, the steric (non-bond) item is more influential than the internal item, which consists with our discussion described above. Though VDW energy is contrary to the changes total energy magnitude, it is also very small, while the magnitude of electrostatic energy decides the magnitude of non-bond energy and then decides the magnitude of total energy.

5. Conclusion

Based on investigations above, we come to the conclusions as: first, for racemic D,L-$[Co(phen)_2$-dpq$]^{3+}$–DNA interactions, the selective intercalations of metal complex to the DNA base stack with dpq as intercalator were observed. In addition, dpq ligand participates the base stack after intercalation. Second, the recognition courses show obvious enantio-selectivity, site-specificity and groove-selectivity. L-$[Co(phen)_2$dpq$]^{3+}$ recognizes pyrimidine–purine/purine–pyrimidine region, especially CG/GC sequence, while the other isomer recognizes the pyrimidine–pyrimidine/purine–purine region, especially TC/AG sequence. When racemic complex interacts with ODN d(GTCGAC)$_2$, L-isomer will be enriched. Third, the static is finally crucial factor during the course of interactions between racemic D,L-$[Co(phen)_2$-dpq$]^{3+}$ and DNA.

We studied the interactions between racemic $[Co(phen)_2$dpq$]^{3+}$ and ODN through NMR methodologies

and molecular simulations. The NMR investigations confirm the reliability of simulation studies and the theoretical work clarifies lots of properties difficulty investigated by experiment alone. Especially, it points out the enantioselectivity of interactions and explains the binding mechanism in detail. Overall, the work offers a feasible method to investigate the interactions between racemic metal complex and oligonucleotide.

Acknowledgments

The authors are grateful to the National Natural Science Foundation of China (Grant No. 20171031) and Provincial Natural Science Foundation of Shanxi for their financial support for this project. The authors wish to express their most sincere appreciation to Caixia Yuan and Vice Prof. Fei Gao, who do the revision for them and Dr. Daxiong Han, who helps them with theoretical work. Tremendous thanks are owned to *State Key Laboratory of Coordination Chemistry of Nanjing University* for helping them with NMR works.

Appendix A. Supplementary data

Supplementary data associated with this article can be found, in the online version, at doi:10.1016/j.jinorgbio.2005.02.008.

References

[1] K.E. Erkkila, D.T. Odom, J.K. Barton, Chem. Rev. 99 (1999) 2777–2795.
[2] D.F. Qi, C.M. Tann, D. Haring, M.D. Distefano, Chem. Rev. 101 (2001) 3081–3111.
[3] A.E. Friedman, C.V. Kumar, N.J. Turro, J.K. Barton, Nucl. Acid Res. 19 (10) (1991) 2595–2602.
[4] C. Turro, S.H. Bossmann, Y. Jenkins, J.K. Barton, N.J. Turro, J. Am. Chem. Soc. 117 (1995) 9026–9032.
[5] B.H. Yun, J.O. Kim, B.W. Lee, P. Lincoln, B. Norden, J.M. Kim, S.K. Kim, J. Phys. Chem. B 107 (2003) 9858–9864.
[6] K. Gisselfalt, P. Lincoln, B. Norden, M. Jonsson, J. Phys. Chem. B 104 (2000) 3651–3659.
[7] J.K. Barton, A.L. Raphael, J. Am. Chem. Soc. 106 (1984) 2466–2468.
[8] B.A. Jackson, V.Y. Alekseyev, J.K. Barton, Biochemistry 38 (1999) 4655–4662.
[9] J.G. Collins, A.D. Sleeman, J.R. Aldrich-Wright, I. Greguric, T.W. Hambley, Inorg. Chem. 37 (1998) 3133–3141.
[10] E.M. Proudfoot, J.P. Mackay, P. Karuso, Biochemistry 40 (2001) 4867–4878.
[11] P.K. Bhattacharya, H.J. Lawson, J.K. Barton, Inorg. Chem. 42 (2003) 8811–8817.
[12] C.M. Dupureur, J.K. Barton, J. Am. Chem. Soc. 116 (1994) 10286–10287.
[13] J.G. Collins, J.R. Aldrich-Wright, I.D. Greguric, P.A. Pellegrini, Inorg. Chem. 38 (1999) 5502–5509.
[14] C.M. Dupureur, J.K. Barton, Inorg. Chem. 36 (1997) 33–43.
[15] J.P. Rehmann, J.K. Barton, Biochemistry 29 (1990) 1701–1709.
[16] Mudasir, N. Yoshioka, H. Inoue, J. Inorg. Biochem. 77 (1999) 239–247.
[17] J. Lan, P. Yang, Microchem. J. 58 (1998) 144–150.
[18] Y. Xiong, L.N. Ji, Coordin. Chem. Rev. 185–186 (1999) 711–733.
[19] J. Lan, P. Yang, Chem. Res. Chin. Univ. 14 (1) (1998) 12–16.
[20] Y.F. Song, P. Yang, Polyhedron 20 (2001) 501–506.
[21] H.L. Chen, P. Yang, Chin. J. Chem. 20 (6) (2002) 1529–1535.
[22] J.G. Collins, T.P. Shields, J.K. Barton, J. Am. Chem. Soc 116 (1994) 9840–9846.
[23] P. Yang, D.X. Han, Sci. China Ser. B 43 (5) (2000) 516–523.
[24] Z.H. Xiong, P. Yang, J. Mol. Struct. (Theochem) 620 (2003) 129–138.
[25] Z.H. Xiong, P. Yang, Chem. J. Chin. Univ. 23 (2002) 57–63.
[26] Z.H. Xiong, P. Yang, J. Mol. Struct. (Theochem) 582 (2002) 107–117.